online data

The crystal structure of the pentahaem *c*-type cytochrome NrfB and characterization of its solution-state interaction with the pentahaem nitrite reductase NrfA

Thomas A. CLARKE*, Jeffrey A. COLE†, David J. RICHARDSON*[1] and Andrew M. HEMMINGS*‡[1]

*Centre for Metalloprotein Spectroscopy and Biology, School of Biological Sciences, University of East Anglia, Norwich NR4 7TJ, U.K., †School of Biosciences, University of Birmingham, Edgbaston, Birmingham B15 2TT, U.K., and ‡School of Chemical Sciences and Pharmacy, University of East Anglia, Norwich NR4 7TJ, U.K.

NrfB is a small pentahaem electron-transfer protein widely involved in the respiratory reduction of nitrite or nitric oxide to ammonia, processes that provide energy for anaerobic metabolism in many enteric bacteria and also serve to detoxify these reactive nitrogen species. The X-ray crystal structure of *Escherichia coli* NrfB is presented at 1.74 Å (1 Å = 0.1 nm) resolution. The architecture of the protein is that of a 40 Å 'nanowire' in which the five haems are positioned within 6 Å of each other along a polypeptide scaffold. During nitrite reduction, the physiological role of NrfB is to mediate electron transfer to another pentahaem protein, NrfA, the enzyme that catalyses periplasmic nitrite or nitric oxide reduction. Protein–protein interaction studies suggest NrfA and NrfB can form a 20-haem $NrfA_2$–$NrfB_2$ hetero-tetrameric complex.

Key words: ammonification, cytochrome, electron transport, nitric oxide, nitrite reductase, protein–protein interaction.

INTRODUCTION

A key reaction in the metabolism of *Escherichia coli* and related enteric pathogens, including *Salmonella enterica*, is the reduction of nitrite to ammonium that is catalysed by cytochrome *c* nitrite reductase (NrfA). This anaerobic respiratory reaction is coupled to the conservation of energy and so contributes to the survival of enteric bacteria in low-oxygen environments, such as those of the gut. In addition to the six e^- reduction of nitrite, NrfA can catalyse the five e^- reduction of nitric oxide to ammonium, and a physiological role for the reduction of nitric oxide in the detoxification of this cytotoxin has been suggested for *E. coli* [1]. The crystal structure of *E. coli* NrfA has been solved [2], along with those of the homologous enzymes from *Sulfurospirillium deleyianum* [3], *Wolinella succinogenes* [4] and *Desulfovibrio desulfuricans* [5]. In all cases, the structure of NrfA is that of a ~110 kDa homodimer with a total of five closely packed haems per monomer. In contrast with the biochemical conservation of NrfA, there are two biochemically distinct systems by which electrons required for nitrite and nitric oxide reduction are transferred through the respiratory electron-transfer system to NrfA [6]. In δ- and ε-proteobacteria, such as *W. succinogenes* and *S. deleyianum*, the electron donor to NrfA is the membrane-bound tetrahaem NrfH [6,7]. This forms a membrane-anchored NrfH–NrfA complex on the periplasmic face of the cytoplasmic membrane that has recently been resolved structurally from *Desulfovibrio vulgaris*, where it was shown to form a complex comprising two NrfH and four NrfA molecules [8]. In contrast, in enteric γ-proteobacteria, such as *E. coli* and *S. enterica*, the direct electron donor to NrfA is NrfB, a water-soluble 21 kDa pentahaem protein [9]. NrfB does not co-purify with NrfA, and so, unlike the stable $NrfA_4$–$NrfH_2$ complex, the NrfA–NrfB complex is an example of a transient, rather than a stable, electron-transfer complex. In the present paper, we show the first structure of NrfB in conjunction with data from solution-state studies on the interaction with NrfA, demonstrating that it forms a $NrfA_2$–$NrfB_2$ complex which must be biochemically distinct from the $NrfA_4$–$NrfH_2$ complex.

EXPERIMENTAL

Purification of NrfB and NrfA

NrfB was prepared using a method modified from that of [9]. The plasmid pNRFB6 was transformed into *E. coli* JM109 cells containing the pEC86 plasmid and grown overnight at 37 °C on LB (Luria–Bertani) agar plates containing 100 $\mu g \cdot ml^{-1}$ carbenicillin and 30 $\mu g \cdot ml^{-1}$ chloramphenicol. Colonies were used to inoculate 5 ml of LB medium containing 100 $\mu g \cdot ml^{-1}$ carbenicillin, 30 $\mu g \cdot ml^{-1}$ chloramphenicol and were grown for 8 h at 37 °C with shaking. Cultures in 1 litre of LB medium containing 100 $\mu g \cdot ml^{-1}$ carbenicillin and 30 $\mu g \cdot ml^{-1}$ chloramphenicol were inoculated with the 5 ml cultures and grown overnight at 37 °C with shaking. Cells were harvested by centrifugation at 9000 ***g*** for 15 min, resuspended in 50 mM Tris/HCl (pH 7.0) and 1 mM EDTA, broken by the French press method and centrifuged at 3000 ***g*** for 45 min to remove membrane fragments. NrfB in the supernatant was precipitated in 30 % (w/v) ammonium sulfate at 4 °C and then resuspended in and dialysed against 50 mM Tris/HCl (pH 7.0). The dialysed NrfB was loaded on to a 2.5 cm × 20 cm Q-Sepharose Fast Flow column (GE Healthcare) equilibrated with 50 mM Tris/HCl (pH 7.0) and eluted using a 250 ml gradient of 0–1 M NaCl. Fractions containing NrfB were identified spectrophotometrically as having

Abbreviations used: AUC, analytical ultracentrifugation; DLS, dynamic light scattering; HAO, hydroxylamine oxidoreductase; LB, Luria–Bertani; NrfA, cytochrome *c* nitrite reductase; NrfB, pentahaem electron donor to NrfA; rmsd, root mean square deviation; SAD, single-wavelength anomalous dispersion; STC, small tetrahaem cytochrome *c*.

[1] Correspondence may be addressed to either of these authors (email d.richardson@uea.ac.uk or a.hemmings@uea.ac.uk).

The structural co-ordinates for the oxidized and reduced NrfB proteins have been deposited in the Protein Data Bank under codes 2OZY and 2P0B respectively.

Table 1 Data for collection and refinement statistics for oxidized and reduced NrfB

Values in parentheses indicate the highest resolution shell. $R = |F_o - F_c|/F_o$. R_{cryst} is calculated with the 95 % of data used during refinement. R_{free} is calculated with a 5 % subset of data not used during refinement.

	SAD data	Oxidized	Reduced
Data collection			
Wavelength (Å)	1.722 Å	0.976 Å	0.976 Å
Resolution (Å)	65–3.0 (3.16–3.0)	44–1.74 (1.83–1.74)	44–1.74 (1.83–1.74)
Unique reflections	4106 (551)	19836 (2915)	19070 (2846)
Completeness (%)	98.6 (93.9)	97.4 (99.3)	94.0 (97.0)
Anomalous completeness (%)	98.4 (92.7)	–	–
R_{sym} (%)	12.6 (22.1)	12.2 (45.0)	13.1 (43.3)
$\langle I/\sigma \rangle$	13.9 (6.8)	4.8 (1.6)	4.7 (1.5)
Multiplicity	6.8 (6.0)	2.8 (2.7)	4.2 (4.0)
Anomalous multiplicity	3.8 (3.3)	–	–
Average atomic B-factor ($Å^2$)	42.3	11.2	8.5
Refinement			
R_{cryst}		6.9 (24.9)	15.9 (20.4)
R_{free}		0.4 (29.7)	19.2 (30.0)
Model			
Protein atoms		1159	1153
Water		198	184
Haem atoms		215	215
Bond length rmsd (Å)		0.013	0.012
Bond angle rmsd (°)		1.50	1.51
Average B-factor ($Å^2$)		13.7	10.9

an A_{410}/A_{280} ratio greater than 1. NrfB-containing fractions were loaded on to a 5/50 Fast Flow Phenyl Sepharose column (GE Healthcare) equilibrated with 50 mM Tris/HCl (pH 7.0) and 100 mM NaCl, and were eluted with a 100 ml gradient of 0–30 % (v/v) propan-2-ol and 10 mM Tris/HCl (pH 7.0). Fractions of 3 ml containing NrfB with an A_{410}/A_{280} ratio greater than 5 were pooled and dialysed into 50 mM sodium Hepes (pH 7.5). As a final purification step, NrfB was passed through a Superdex 75 16/60 gel-filtration column (GE Healthcare) equilibrated with 50 mM sodium Hepes (pH 7.5). NrfB eluting from the gel-filtration column was judged to be pure by Coomassie Blue-stained SDS/PAGE gels and a A_{410}/A_{280} ratio greater than 9. NrfA was prepared from *E. coli* K-12 strain LCB2048 [10] and purified according to established procedures [2]. The turnover number of purified NrfA was 800 NO_2^- s^{-1} at 25 °C and the NrfA concentration (unless otherwise stated, the concentration of NrfA refers to the total concentration of the 53 kDa NrfA subunit) was determined using an ε_{410} of 497 $mM^{-1} \cdot cm^{-1}$, based on a monomeric molecular mass of 53 kDa.

Crystallization of NrfB, data collection and processing

Purified NrfB was concentrated to 8 $mg \cdot ml^{-1}$ and centrifuged at 16000 ***g*** for 10 min at 4 °C before crystallization. Crystals were obtained by the vapour-diffusion method under anaerobic conditions using 250 mM trisodium citrate, 10 mM $Na_2S_2O_4$ and 20 % (v/v) propan-2-ol in 100 mM sodium Hepes, pH 7.5. Oxidized crystals were prepared by moving trays containing fully formed crystals to an aerobic environment at 4 °C for 24 h before harvesting. Crystals were judged to be oxidized on the basis of the colour change that occurs to cytochromes when becoming oxidized or reduced. For data collection, crystals were soaked with a solution of reservoir buffer containing 20 % (v/v) ethylene glycol as a cryoprotectant. The oxidized absorbance spectrum of NrfB has peaks at 410 and 530 nm that are typical of *c*-type cytochromes [9]. On reduction, the 410 nm peak decreases and is replaced by peak a 420 nm, while the 530 nm peak is split into two peaks at 520 and 550 nm. This spectral change can be visualized as a colour change from orange–red to pink–red. NrfB crystals typically had approximate dimensions of 10 μm × 10 μm × 100 μm and were too small to be analysed spectrophotometrically. However, crystals of reduced NrfB were prepared by soaking the oxidized crystals for 1 min in oxygen-free reservoir solution with 20 % (v/v) ethylene glycol and 50 mM $Na_2S_2O_4$ until the orange–red to pink–red colour change was observed, indicating reduction, and then immediately plunged into liquid nitrogen. To ensure that reducing conditions were maintained, the reducing solution was tested after each crystal was harvested using strips of filter paper soaked in 100 mM Methyl Viologen.

X-ray diffraction datasets were measured using an ADSC detector on beamline ID29 at the ESRF (European Synchrotron Radiation Facility, Grenoble, France). The NrfB crystals used for data collection were all of space group $P2_12_12_1$ and were essentially isomorphous with typical cell dimensions $a = 49.7$ Å (1 Å = 0.1 nm), $b = 59.7$ Å and $c = 65.2$ Å. Assuming one molecule of NrfB in the crystallographic asymmetric unit, the solvent content of the crystals was approx. 45 % (v/v). Owing to the small size of the NrfB crystals, we were unable to measure an iron K-edge absorption spectrum and so instead collected a SAD (single-wavelength anomalous dispersion) dataset near the presumed iron K-edge at a wavelength of 1.722 Å to a resolution of 3.0 Å. Further diffraction datasets for both oxidized and dithionite-reduced NrfB were obtained from single crystals to a resolution of 1.74 Å using an X-ray wavelength of 0.976 Å. All datasets were processed using MOSFLM [11] and SCALA [12] as part of the CCP4 package [13]. Data collection statistics are summarized in Table 1.

Structure determination and refinement

The structure of NrfB was determined by SAD phasing methods using the anomalous signal originating from the five haem iron atoms present in the single molecular copy of NrfB present in the asymmetric unit. Identification of the iron atom sites and subsequent phasing at 3.5 Å resolution was performed using

SHELX [14]. An electron density map calculated with these phases allowed manual building of haems 1, 3, 4 and 5 and 45 % of the amino acid backbone using COOT [15]. Phases were improved using the partial model and extended to 3.0 Å resolution with SHARP [16], allowing 66 % of the amino acid backbone to be built. The phases from the SAD dataset were extended to 2.5 Å using the oxidized NrfB dataset. Following four rounds of simulated annealing refinement at 2.5 Å resolution against the oxidized NrfB data using CNS [17], an improved map was obtained which allowed haem 2, the amino acid side chains and an additional 9 % building of the amino acid chain to be added to the structural model. Subsequent rounds of simulated annealing and manual intervention using COOT gave a model containing all five haems and 141 amino acids (86 % of the total) corresponding to NrfB residues 19–160 (unless stated otherwise, the amino acid numbering refers to the processed protein without the signal peptide, which is experimentally determined to start at position 26 on the pre-protein sequence). This interim structural model had an R_{cryst} (R_{free}) of 28.4 % (32.5 %) using data in the resolution range 65–2.5 Å. In all cases, the R_{free} value provided refers to an R-value calculated using 5 % of the data selected randomly and otherwise excluded from refinement [18]. The final refined structure of oxidized NrfB was obtained by alternating rounds of manual model building and automatic refinement using REFMAC [19] against all data to 1.74 Å resolution. This gave a structural model containing all five haems and residues 19–160 having an R_{cryst} (R_{free}) of 22.1 % (24.8 %) for data in the resolution range 60–1.74 Å. Addition of 198 water molecules using ARP [20] gave a final structure with an R_{cryst} (R_{free}) of 16.9 % (20.4 %) for data in the same resolution range. When analysed for stereochemical quality using PROCHECK [21], the structure has 90.9 % of residues in the most favoured regions of the Ramachandran plot with the remainder falling into additional allowed regions.

The structure of reduced NrfB was determined by molecular replacement using the final oxidized NrfB structure as a search model, but lacking water molecules [22]. This was corrected by cycles of manual model building and automatic refinement in the same fashion as used for the structure of the oxidized protein. After addition of 184 water molecules the refined structure had an R_{cryst} (R_{free}) of 15.9 % (19.2 %) for data in the resolution range 65–1.74 Å. The structure has 90.9 % of the residues in the most favoured regions with the remainder in additional favoured regions. As with oxidized NrfB, the final model for the reduced protein also lacks the N-terminal 18 residues and four residues from the C-terminus. N-terminal sequencing (Protein and Nucleic Acid Chemistry Facility, University of Cambridge, Cambridge, U.K.) of the soluble expressed protein showed that the NrfB signal peptide is cleaved after position 25 of the protein sequence predicted from the DNA sequencing (see Supplementary Figure S1 at http://www.BiochemJ.org/bj/406/bj4060019add.htm). The residues of the N-terminus point towards the solvent cavity in the crystal lattice, suggesting that these residues are flexible and disordered in the NrfB crystal structure.

Estimation of the hydrodynamic radii of NrfA and NrfB

The hydrodynamic radius of NrfA in solution was measured using DLS (dynamic light scattering). Samples (20 μl) of 5–40 μM NrfA in 50 mM sodium Hepes (pH 7.0) and 2 mM $CaCl_2$ were centrifuged at 10000 ***g*** for 10 min to remove dust and large aggregates. Samples (12 μl) were then pipetted into a sample cell and analysed at 20 °C using a Dynapro-MSX-TC equipped with a 50 mW 843 nm solid-state laser (Protein Solutions). The hydrodynamic radius of NrfB in 50 mM sodium Hepes (pH 7.5) and 1 mM CHAPS was measured in an identical manner. Two sets of data, each with more than 20 readings, were taken at various concentrations and analysed, and the hydrodynamic radii obtained using DYNAMICS version 5.0 software. The molecular mass at each concentration was determined from the hydrodynamic radius by reference to the standard curve method in the software.

Titration of the NrfA–NrfB complex using UV–visible absorbance and fluorescence emission spectroscopy

Absorbance measurements were performed on a Hitachi V-3310 dual-beam spectrophotometer; the sample cuvette contained 50 mM sodium Hepes (pH 7.0), 2 mM $CaCl_2$ and 1.7 μM NrfA, while the reference cuvette contained an equal volume of 50 mM sodium Hepes (pH 7.0) and 2 mM $CaCl_2$. After allowing the cuvettes to equilibrate to 20 °C for 5 min, 15 scans of the NrfA spectrum were recorded in the wavelength range 250–600 nm. Aliquots of a 200 μM NrfB solution were added to the sample and reference cuvettes. The cuvettes were then left to equilibrate for 15 min before a further 15 scans were recorded. Each set of scans were averaged, and the NrfB spectrum was subtracted from the NrfA + NrfB spectrum to obtain a difference spectrum caused by a change in the environment of a haem owing to complex formation. The dissociation constant of the NrfA–NrfB complex was determined by fitting the obtained data to eqn (1) using the program TABLECURVE (Systat software).

$$A = A_0\left(\frac{[\mathrm{NrfA}] + [\mathrm{NrfB}] + K_d^{AB}}{2} - \sqrt{\frac{\left([\mathrm{NrfA}] + [\mathrm{NrfB}] + K_d^{AB}\right)^2}{4} + [\mathrm{NrfA}][\mathrm{NrfB}]}\right) \quad (1)$$

where A is the observed spectral change, A_0 is the maximum theoretical spectral change, [NrfA] is the concentration of monomeric NrfA, [NrfB] is the concentration of the monomeric NrfB, and K_d^{AB} is the dissociation constant of the NrfA–NrfB complex.

A PerkinElmer LS50B fluorimeter equipped with a temperature-controlled water bath at 20 °C was used for fluorescence emission spectroscopy measurements. The excitation wavelength was 295 nm with a 5 nm bandwidth, and the emission wavelength measured was 348 nm with a 12.5 nm bandwidth. For each measurement, the average of 30 scans was taken. A fluorescence cuvette containing 2 ml of 50 mM sodium Hepes (pH 7.0) and 2 mM $CaCl_2$ was used to measure a baseline. A sample of either NrfA or NrfB was then added, and the change in fluorescence was measured. Experiments were performed in triplicate. For experiments analysing complex formation, 1.8 μM NrfB was added to the cuvette and the baseline was measured, sequential additions of NrfA were then added to give a final concentration between 0.045 and 0.32 μM. The overall change in fluorescence was recorded between each addition.

AUC (analytical ultracentrifugation)

AUC experiments were performed using a Beckman XLI analytical ultracentrifuge equipped with absorbance optics. The partial specific volumes of NrfA and NrfB were calculated from the amino acid sequence using SEDNTERP (version 1.05) (http://www.jphilo.mailway.com/) and had values of 0.735 and 0.715 $ml \cdot g^{-1}$ respectively. All experiments were performed in the presence of 50 mM sodium Hepes (pH 7.0) and 2 mM $CaCl_2$

using either NrfA or an equimolar mixture of NrfA and NrfB at a range of different concentrations. Sedimentation equilibrium experiments were performed at 9000 rev./min at 20 °C using a Beckman Ti-50 rotor, using 2, 10 or 20 μM oxidized NrfA to measure the dissociation constant of the NrfA monomer–dimer equilibrium. The concentration profiles of NrfA during analytical ultracentrifugation were measured at 410, 440 and 530 nm for 2, 10 or 20 μM NrfA respectively. Scans were recorded every 4 h to determine when protein samples had reached equilibrium in the centrifuge. When equilibrium had been achieved, ten scans were recorded for each sample. The program Ultrascan II [23] was used to fit the obtained sedimentation equilibrium profiles to both single species models, as well as monomer–dimer equilibrium models where the NrfA monomer and dimeric states are in a dynamic equilibrium and the NrfA monomer has a molecular mass of 53 kDa.

To measure the dissociation constant of the NrfA–NrfB complex, a stock equimolar mixture of NrfA and NrfB at 20 μM was prepared using the molar absorption coefficients of the haem peaks of both NrfA and NrfB [2,9]. Equilibrium experiments were executed at 7500 and 9000 rev./min at 20 °C using a Beckman Ti-50 rotor, using concentrations of 1, 5 and 20 μM NrfA and NrfB. The concentration profiles of the NrfA–NrfB complex were measured at 410, 530 and 600 nm for 1, 5 and 20 μM NrfA respectively. When equilibrium was achieved, ten scans were recorded for each sample. When fitting all six datasets simultaneously, only three scans for each dataset were used. The data were fitted as before to obtain sedimentation equilibrium profiles to both single species models and monomer–dimer equilibrium models where the NrfA–NrfB heterodimer and $NrfA_2$–$NrfB_2$ heterotetramer are in a dynamic equilibrium and the NrfA–NrfB dimer has a molecular mass of 74 kDa. The S.D. values shown are obtained by measuring the S.D. of the equilibrium constants measured using only one scan for each dataset.

RESULTS

The 1.7 Å crystal structure of NrfB

The overall structure of the NrfB polypeptide is unique among multihaem *c*-type cytochromes. The approximate overall dimensions are 40 Å × 30 Å × 20 Å, with a chain of five haems distributed through the structure (Figures 1A and 1C). The maximum edge-to-edge distance of the haem porphyrin rings is 40 Å, and the propionate side chains of all five haems are solvent-exposed. The first observed residue at the N-terminus of the crystal structure is Asn^{19}, and the polypeptide chain is continuous for 142 residues until Lys^{160} near the C-terminus of the chain of the processed protein. A haem group is covalently attached approximately every 20–25 amino acids via thiol ester linkages to the cysteine residues of five classical CXXCH attachment sites (Figure 2A), so that all five of the minimum inter-porphyrin ring distances between neighbouring haems lie within 6 Å. A total of 35 % of the protein chain is folded in an α-helical manner, and the remainder is extended loop regions that serve to connect the chain of haem groups (Figure 1A). The haems are arranged in a series of alternative parallel and perpendicular pairs (Figure 1B) so that there are two parallel pairs (haems 1,2 and haems 3,4) and two perpendicular pairs (haems 2,3, and haems 4,5). Owing to the close packing of the haems, the porphyrin rings of haem 2 and haem 4 are only separated by a distance of 11 Å, making it possible, in principle, for electron transfer to bypass haem 3 (Figure 1A). It is notable that, in making this arrangement, each set of adjacent parallel and perpendicular haem pairs can be superimposed on to each other so that haems 1,2 can be superimposed on to haems 3,4 with an rmsd (root mean square deviation) of 0.39 Å. The two haem elbow motifs comprising haems 2,3 and haems 4,5 can also be superposed with an rmsd of 1.4 Å, where the iron atoms of each haem are directly superimposable and the increase in rmsd is caused by slight changes in the relative angle of the haems. This reflects the conservation of these haem-pairing arrangements, which is maintained despite quite different protein loops connecting the haem pairs in the two halves of the protein (Figure 1A). It is also possible to superimpose haem triads, such that haems 1,2,3 can be superimposed on to haems 3,4,5 with an rmsd of 1.9 Å (Figure 1D). The other two potential haem triad combinations, superimposing haems 1,2,3 with haems 2,3,4, or haems 2,3,4 with 3,4,5, have much higher rmsd (5.3 and 3.8 Å respectively). This is due to the difference in the position of the parallel haem pairs compared with the position of the haem elbow.

There are only a few significant changes between the structure derived from untreated air-oxidized crystals and that derived from crystals pre-reduced with dithionite immediately before data collection (Figure 1C). The α-carbons of the main chain backbones of NrfB deviate with an rmsd of only 0.20 Å. However, two loops containing residues 21–30 and 106–112 have rmsd values of 0.46 and 0.70 Å respectively. Both loops are on the molecular surface close to haems 2 and 3 (Figure 1C), and the change in the NrfB crystal structure is best described as a slight contraction in the surface of the protein near haems 2 and 3. The propionate groups of the haems are also changed slightly in position, most significantly in haem 5, where one propionate group moves closer to the haem iron.

All five haem iron ions are axially co-ordinated by two histidine ligands. The resolution of the electron-density map is sufficient to identify the orientation of the imidazole rings with respect to the haem-iron ligand (Figure 1E). The imidazole planes of the two ligands are either near-parallel or twisted into a more perpendicular arrangement (Figure 1B). Previous studies showed that the EPR spectrum of purified oxidized NrfB exhibited two main features: a rhombic signal at 2.99, 2.27 and 1.5 that was attributed to low-spin haems, where the histidine imidazole rings were near-parallel, and a weak 'large g_{max}' signal with a *g*-value of 3.57 attributed to haems where the imidazole rings were in a near-perpendicular arrangement [9]. The 'large g_{max}' EPR signal is well documented [24] and results from the near-degenerate state of the d_{xz} and d_{yz} orbitals, which is caused by the perpendicular arrangement of the planar imidazole rings. In contrast, the near-parallel arrangement of imidazole rings results in a difference in energy between the d_{xz} and d_{yz} orbitals which results in a rhombic EPR signal. Quantification of the rhombic and large g_{max} signals gave values of 2 spin · $NrfB^{-1}$ and 3 spin · $NrfB^{-1}$ respectively, in complete agreement with the orientation of the imidazole ring planes observed in the crystal structure. Each proximal ligand is contributed by the CXXCH motif that anchors it to the protein, and each distal ligand arises from one of the five histidine residues that are conserved throughout the NrfB family of proteins (Figure 2A). The histidine axial ligands provide important determinants to the final folding with the following pairings: His^{64}–His^{28}; His^{57}–His^{120}; His^{92}–His^{39}; His^{117}–His^{104} and His^{142}–His^{107} (Figure 2). These histidine residues are completely conserved throughout the NrfB family, suggesting that NrfB proteins from different bacteria share a common structure. It is possible that the distal histidine ligands are important for protein stability, as they are clustered on one side of the protein which is predominantly composed of loops.

The C-terminal haem 5 is the most solvent-exposed of all the haems, contributing 300 $Å^2$ of the surface of the protein (Figure 2B). The next most exposed is the N-terminal haem 1, contributing 216 $Å^2$. The surface exposures of the middle

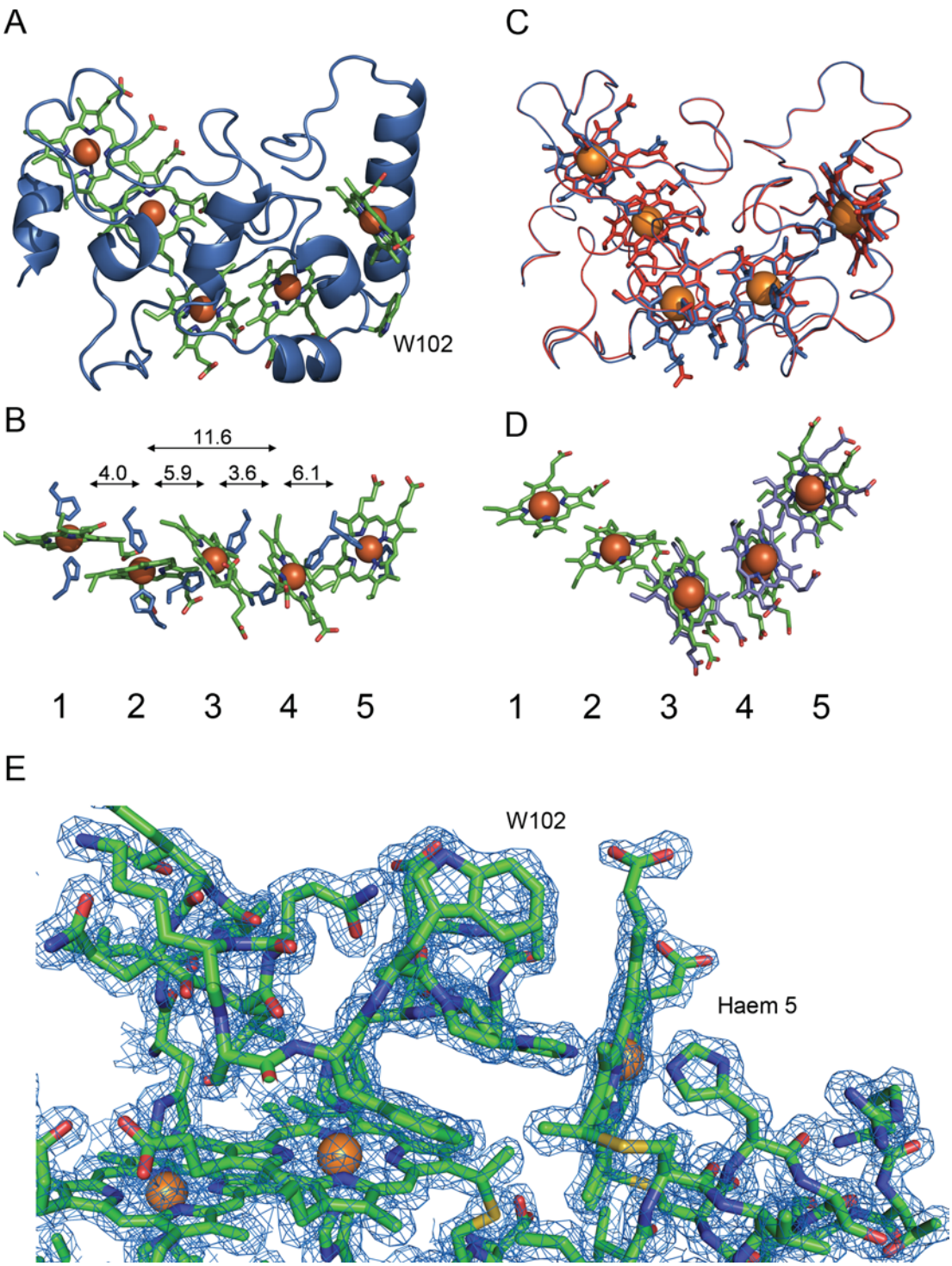

Figure 1 Crystal structures of NrfB

All Figures showing protein structures were prepared using PyMOL (DeLano Scientific). (**A**) The crystal structure of *E. coli* NrfB represented as the α-carbon trace with five haems and Trp^{102} displayed in green. (**B**) Haem organization within NrfB, histidine side chains are shown in blue. The distances (in Å) between haems are shown above; the haem numbers are shown underneath. (**C**) Superimposition of the oxidized and reduced haem structures. The α-carbon trace and haems of the oxidized and reduced enzymes are shown in red and blue respectively. (**D**) Superimposition of haems 1, 2 and 3 (blue) over haems 3, 4 and 5 (green) with an rmsd of 1.9 Å. The haem numbering refers to the green haems. (**E**) Region of the electron-density map contoured at 1.1 σ calculated from the final refined structure of oxidized NrfB in the region of haems 5, 4 and 3 and Trp^{102}. The Figure demonstrates the quality of the fit of the structural model to the map.

haems 2, 3 and 4 are 132, 138 and 140 $Å^2$ respectively. These values suggest routes of electron entry/exit to the NrfB haem-wire via haems 1 and 5. However, the non-negligible solvent exposures of haems 2, 3 and 4 opens up the possibility for electron input or egress at multiple sites in the protein. By mapping the most conserved residues of the NrfB amino acid sequence on to the surface of the *E. coli* NrfB structure, structurally important surface regions can be identified (Figure 2B). The area around haem 5 is

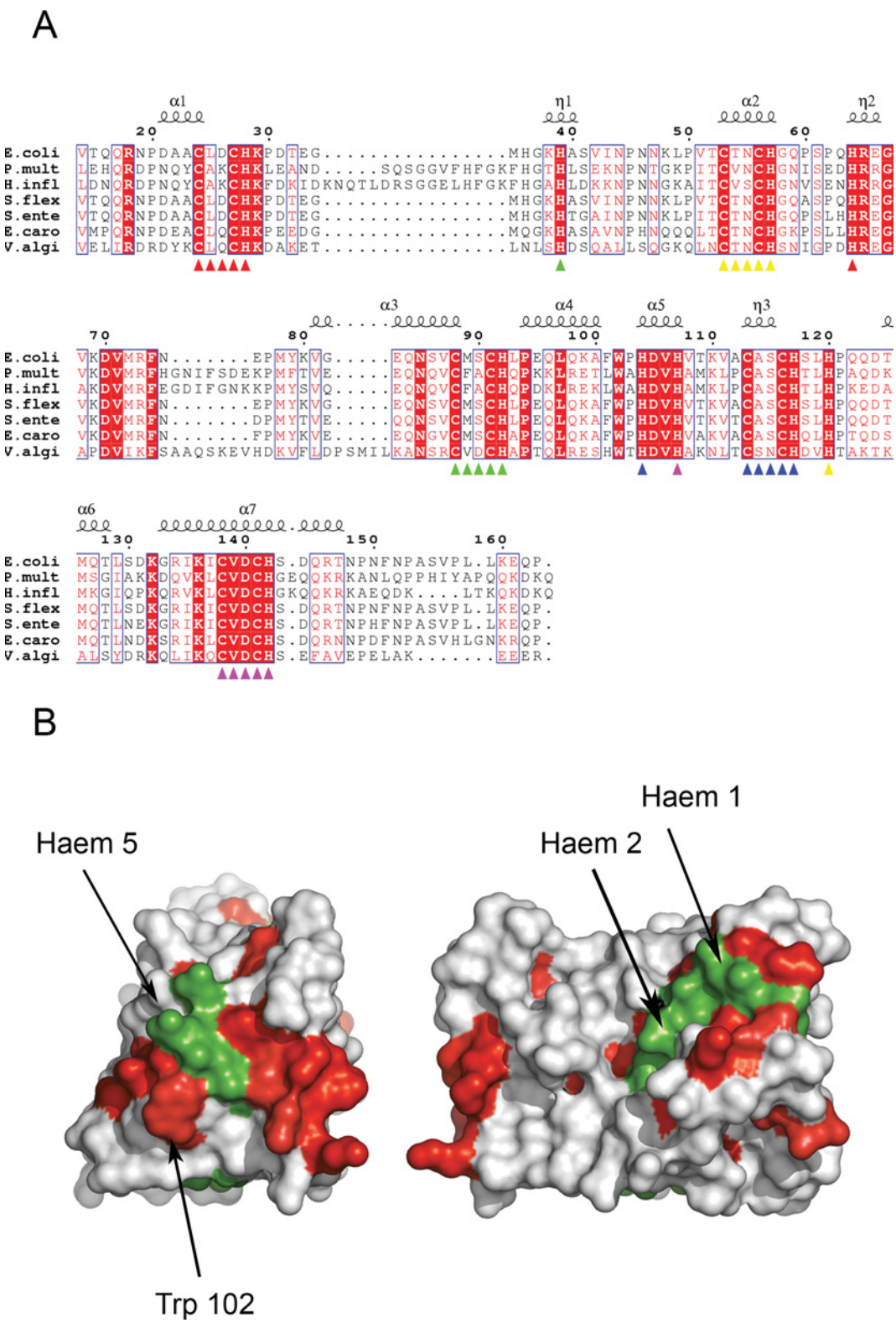

Figure 2 Amino acid sequence conservation in NrfB primary and tertiary structures

(**A**) An amino acid sequence alignment of *E. coli* NrfB (residues 14–163) with NrfBs from *Pasteurella multocida* (P.mult), *Haemophilus influenzae* (H.infl), *Shigella flexneri* (S.flex), *Salmonella enterica* (S.ente), *Erwinia carotovora* (E.caro) and *Vibrio alginolyticus* (V.algi). Red-filled boxed amino acids are identical in the alignment, unfilled boxed amino acids are similar in the alignment. The secondary structure of *E. coli* NrfB is indicated above the sequence alignment. The CXXCH motifs are indicated by coloured triangles under the alignment according to: haem 1, red; haem 2, yellow; haem 3, green; haem 4, blue; haem 5, magenta. The corresponding distal histidine residues of each haem are also coloured accordingly. (**B**) Surface map of the side (right-hand panel) and C-terminal end (left-hand panel) of NrfB. Completely conserved residues are shown in red, haems 5, 2 and 1 are shown in green. All other residues are shown in white.

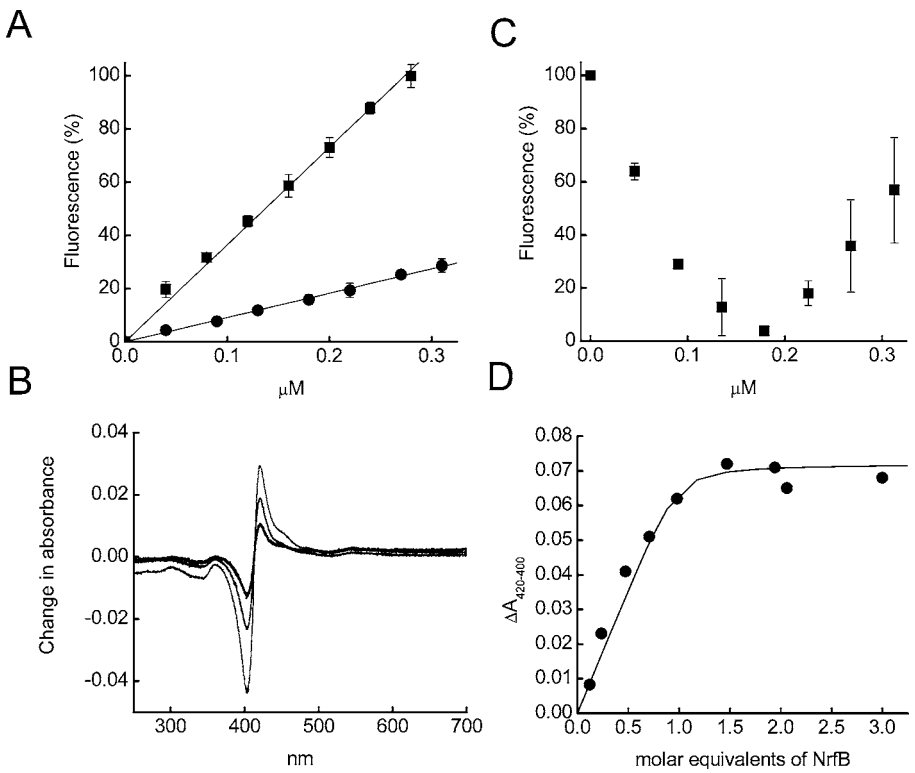

Figure 3 Complex formation between NrfA and NrfB measured by fluorescence and absorption spectroscopy

(**A**) Dependence of the relative fluorescence of NrfB (■) or NrfA (●) on protein concentration. 100 % represents the maximum fluorescence obtained with 0.31 μM NrfB. Results are means ± S.D. for three separate experiments. (**B**) Titration of 0.18 μM NrfB with 0–0.31 μM NrfA. The percentage scale on the *y*-axis represents the change in fluorescence obtained, where 100 % is the maximum observed in the experiment (0.18 μM NrfB in the absence of NrfA) and 0 % is the minimum observed in the experiment (0.18 μM NrfB in the presence of 0.18 μM NrfA). Results are means ± S.D. for three separate experiments. (**C**) Shift in the UV–visible spectrum following addition of 0.4 (—), 0.8 (—) or 2.4 (–)μM NrfB to a solution containing 1.7 μM NrfA. (**D**) The amplitude of the change in absorbance shown in (**C**) plotted as a function of NrfB concentration; the line was fitted iteratively using eqn (1) as described in the Experimental section.

predominantly conserved, suggestive of a potential protein–protein binding site. This region includes an exposed conserved tryptophan residue, Trp^{102} (see below). The next most conserved region is that around the surface of haem 1, suggesting a second potential binding site. This supports the hypothesis that haems 1 and 5 are the likely sites of electron input to or output from NrfB.

The solution-state interaction of NrfB with NrfA

E. coli NrfB contains only one tryptophan residue and this is conserved in NrfB from other bacteria, including *Pasteurella multocida*, *Haemophilus influenzae*, *Shigella flexneri*, *Salmonella enterica*, *Erwinia carotovora* and *Vibrio alginolyticus* (Figure 2A). This tryptophan residue is positioned on the surface near haem 5 in the refined crystal structure (Figures 1A and 2B). The fluorescence of this tryptophan residue can be used to reveal changes in the vicinity of haem 5. The fluorescence of NrfA and NrfB was monitored using an excitation wavelength of 295 nm and the corresponding emission at 348 nm. In control experiments, as the concentration of NrfB increased from 0.05 to 0.28 μM, the fluorescence intensity increased linearly. As the concentration of NrfA increased from 0.05 to 0.31 μM, the fluorescence also increased linearly, although the observed fluorescence was only 20 % that of the NrfB fluorescence at the same concentration. However, when NrfA was added to a fluorescing solution of NrfB, the total observed fluorescence decreased initially (Figure 3B). This decrease continued until NrfA and NrfB were present at equimolar concentrations (0.18 μM in Figure 3B). Further additions of NrfA then led to an increase of fluorescence in a manner expected for the additive effects of free NrfA. This suggests that the two proteins form a complex that leads to a decrease in the fluorescence of the NrfB tryptophan residue. This decrease in fluorescence continued until a NrfA/NrfB ratio of 1.0 was achieved, the fluorescence then increased for a situation in which there is a NrfA–NrfB complex and excess free NrfA, showing that the change in the tryptophan environment is consistent with the formation of an equimolar NrfA–NrfB complex.

UV–visible spectroscopy was also used to study this complex formation. Although NrfA and NrfB have strongly overlapping UV–visible spectra, a small change occurred when increasing amounts of NrfB were added to NrfA and this could be resolved through the use of difference spectra (Figure 3C). It is impossible to attribute this change to a particular protein or haem group as the change is caused by mixing two pentahaem proteins. Control experiments in which NrfB was added to buffer, or buffer added to NrfA, did not cause the observed spectral shift. As the amount of NrfB added increased, the amplitude of the change between 410 and 420 nm increased until the NrfA concentration was equivalent to the NrfB concentration and the amplitude of the spectral change remained constant (Figure 3). This plateau was reached at equimolar concentrations of 0.17 μM NrfA and NrfB in Figure 3(D), and the data were fitted using eqn (1) to give a dissociation constant (K_d^{AB}) of 37 ± 24 nM for the dissociation of a NrfA–NrfB complex with a stoichiometry of 1:1. We recognize that this represents an upper limit, as it is necessary to use concentrations much higher than the dissociation constant to

Table 2 Dynamic light scattering analyses of the dimerization of NrfA and NrfB

Experiments were performed at 20 °C using solutions containing 5–38 μM NrfA or 11–45 μM NrfB in 50 mM sodium Hepes (pH 7.0) and 2 mM $CaCl_2$.

(a)

[NrfA] (μM)	R_H (nm)	Molecular mass (kDa)	Polydispersity (%)
38	4.2 ± 0.2	102 ± 7	29 ± 11
9	4.2 ± 0.2	102 ± 7	51 ± 31
7.5	3.4 ± 0.2	63 ± 9	72 ± 19
5	3.7 ± 0.2	62 ± 13	91 ± 11

(b)

[NrfB] (μM)	R_H (nm)	Molecular mass (kDa)	Polydispersity (%)
11	2.5 ± 0.1	30 ± 6	13 ± 10
21	2.5 ± 0.1	27 ± 6	26 ± 15
45	2.6 ± 0.1	30 ± 6	28 ± 19

observe the subtle change in absorbance. Taken together, the fluorescence and UV–visible studies indicate that NrfB forms a tight stable complex with NrfA with a probable stoichiometry of either 1:1 or, as the crystal structure shows NrfA to be dimeric, 2:2.

Having gained an insight into the stoichiometry of the NrfA–NrfB electron-transfer complex, the effect of NrfB on NrfA self-association was investigated. First, the self-association of air-oxidized NrfA was assessed by measuring the hydrodynamic radius using DLS. The range of measured hydrodynamic radius broadened and the percentage polydispersity decreased as the concentration of NrfA increased (Table 2). A low polydispersity value indicates a homogenous sample. Thus the data suggest that oxidized NrfA was in a dynamic equilibrium of monomer and dimer over the concentration range 5–38 μM and that, as the concentration of NrfA increased, so did the proportion of dimeric NrfA at equilibrium. Estimating the molecular mass of the protein in solution from the hydrodynamic radius measured yielded a value of 102 kDa at NrfA concentrations $\geqslant 9$ μM (Table 2). This is similar to the calculated molecular mass of the $NrfA_2$ complex (106 kDa). However, as the concentration of NrfA decreased below 9 μM, the apparent molecular mass changed to 62 kDa, close to the molecular mass calculated for the NrfA monomer. The sudden decrease in molecular mass observed between 9 and 7.5 μM is probably most likely to be due to small changes in the concentration of monomeric and dimeric species in solution causing artificially large changes in the measured molecular mass distribution, and this is reflected in the increasing polydispersity. DLS analysis of samples of NrfB over a similar concentration range showed that NrfB did not dimerize. The dissociation constant of the NrfA homodimer into its component monomers (K_d^{AA}) was measured using sedimentation equilibrium experiments on air-oxidized NrfA at 2, 10 and 20 μM concentration. The absorbance of the NrfA haem groups was used to measure the concentration of NrfA across the ultracentrifuge cell (note that the haem/protein ratio remains constant regardless of the oligomeric state of the protein, and we established that the absorbance properties were not changed through the monomer–dimer transitions). When NrfA was subjected to centrifugation at 9000 rev./min, a stable concentration gradient across the ultracentrifuge cell was formed after approx. 12 h (Figure 4). This gradient is directly dependent on the averaged molecular mass of NrfA in solution, and this value increased with increasing concentration in a manner similar to that observed in the DLS experiments, confirming that dissociation of the $NrfA_2$ complex occurred over the concentration range 2–20 μM. Ultrascan II [23] was used to simultaneously fit the data at all three concentrations and the best fit to the data (Figure 4A) yielded a K_d of 4.0 ± 0.7 μM for the dissociation of the $NrfA_2$ decahaem complex into pentahaem monomers, this value was consistent with the data obtained from DLS experiments (Table 2).

Sedimentation equilibrium experiments on solutions containing equal amounts of NrfA (53 kDa) and NrfB (21 kDa) at 2, 5 or 20 μM showed that the averaged molecular mass of the NrfA–NrfB sample increased significantly when compared with NrfA alone. The averaged molecular mass in a mixture of 20 μM of each protein (147 ± 9 kDa) was similar to that expected of a 148 kDa $NrfA_2$–$NrfB_2$ heterotetramer (Table 3). The sedimentation equilibrium profiles of the NrfA–NrfB complex (Figure 4B) were simultaneously fitted to a monomer–dimer equilibrium with a NrfA–NrfB heterodimer molecular mass of 74 kDa to yield a dissociation constant of 4.1 ± 0.2 μM for the 2(NrfA–NrfB) ↔ $NrfA_2$–$NrfB_2$ equilibrium. This is similar to the K_d of 4.0 μM obtained for the 2NrfA ↔ $NrfA_2$ equilibrium. The data implies that formation of the $NrfA_2$–$NrfB_2$ complex does not affect the dissociation at the $NrfA_2$ dimer, suggesting that NrfB binds at a site that is remote from this NrfA interface.

DISCUSSION

In the present paper, we have shown the first crystal structure of NrfB, a periplasmic pentahaem electron-transfer protein. NrfB is involved in shuttling electrons from an integral membrane quinol-oxidizing protein complex, NrfC–NrfD, to a pentahaem nitrite reductase (NrfA) and is conserved in many enteric pathogens. We have presented two crystal structures of NrfB, one derived from data collected from crystals that were in an 'air-oxidized' state immediately before exposure to X-rays and another derived from data collected from crystals that were treated with dithionite reductant immediately before exposure to X-ray irradiation. Although the colour of the crystals indicated that the two treatments yielded NrfB haems in different redox states, we recognize that the level of photoreduction that occurs to the 'air-oxidized' NrfB through exposure to X-rays during data collection is not known so that it can not be excluded that both structures represent reduced forms of the protein. Importantly, however, the crystallographically derived co-ordination structure of the five NrfB haems is exactly as predicted from solution and frozen-solution MCD (magnetic circular dichroism) and EPR spectroscopy [9]. These two methods together show that all five ferric haems are low-spin hexaco-ordinate species with bis-histidinyl axial co-ordinate. This is also the case in both crystal structures. Furthermore, the EPR analyses showed that, in three of the NrfB haems, the imidazole rings of the histidine ligands are near-perpendicular, whereas in the remaining two, they are near-parallel. This is also the case in both NrfB crystal structures. This then gives confidence that the co-ordination environment of the NrfB haems in the crystal structures reflects that in solution.

A number of lines of evidence are also presented that suggest NrfA and NrfB form a 1:1 complex in solution. The mass of this complex (~150 kDa), determined by AUC indicate that it is a 20 haem $NrfA_2$–$NrfB_2$ heterotetramer. We have determined previously the structure of NrfA, which crystallizes as a 106 kDa homodimer with a total of ten closely packed haems [2] (see Supplementary Figure S2 at http://www.BiochemJ.org/bj/406/bj4060019add.htm). Four of the haems in each monomer are bis-histidine-ligated, while the active-site haem is ligated by a proximal lysine ligand and, depending whether a substrate such as nitrite or hydroxylamine is included in the crystallization

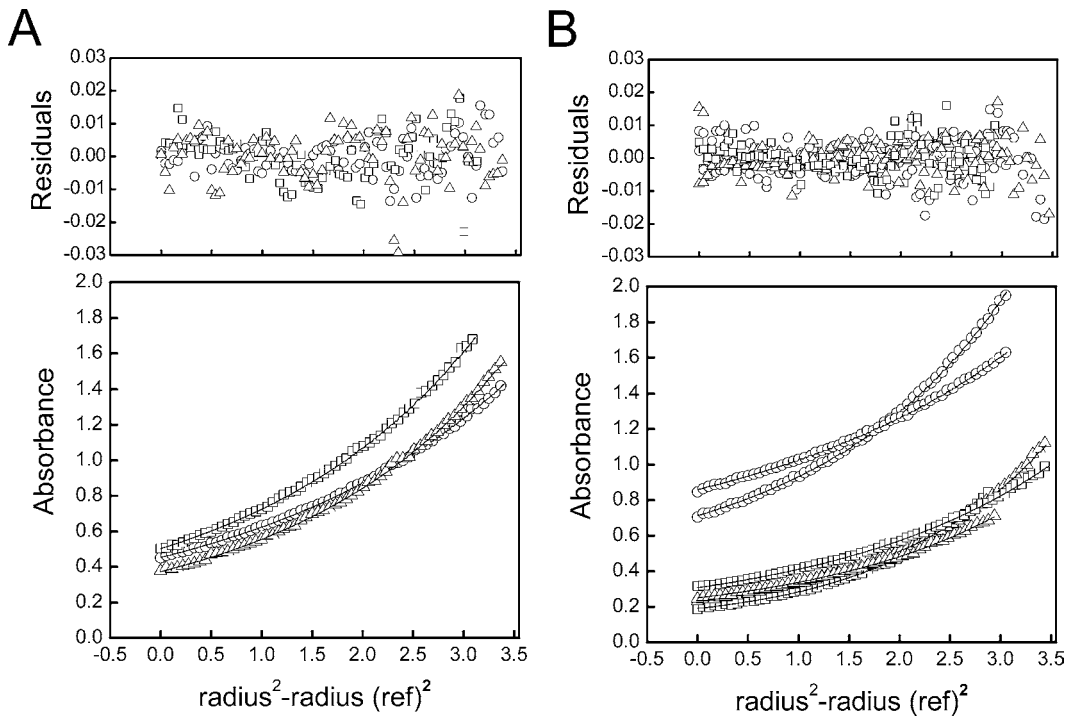

Figure 4 Sedimentation equilibrium analyses of NrfA and NrfB

(**A**) Dissociation of the NrfA dimer in solution as monitored by sedimentation equilibrium. NrfA in 50 mM sodium Hepes (pH 7.0) and 2 mM $CaCl_2$ was centrifuged at 9000 rev./min at 20 °C for 24 h until equilibrium had been achieved. Lower panel: the absorbance profiles of NrfA at 2 (○), 10 (□) and 20 (△) μM were all fitted to a model where the NrfA dimer dissociated into 53 kDa monomers with a K_d^{AA} of 4.0 ± 0.7 μM. Upper panel: residual difference between the experimental data and the fitted curves. (**B**) Dissociation of the $NrfA_2$–$NrfB_2$ tetramer into NrfA–NrfB heterodimers. NrfA–NrfB at 1, 5 and 20 μM was centrifuged at 7500 or 9000 rev./min at 20 °C until equilibrium was achieved. Lower panel: absorbance profiles of the NrfA–NrfB complex at 1 (○), 5 (□) and 20 (△) μM at both 7500 and 9000 rev./min were fitted to a model where the $NrfA_2$–$NrfB_2$ tetramer dissociated into 74 kDa NrfA–NrfB heterodimers with a K_d of 4.1 ± 0.2 μM. Upper panel: residual difference between the experimental data and the fitted curves.

Table 3 Analysis of NrfA and NrfB interactions by AUC

Sedimentation experiments were performed on NrfA, and mixtures of NrfA and NrfB over a range of concentrations using a Beckman XL-I analytical centrifuge. NrfA was centrifuged at 9000 rev./min, while the NrfA–NrfB complex was centrifuged at 7500 and 9000 rev./min. Scans were collected every 4 h until equilibrium was achieved. The averaged molecular mass was determined for each sample using Ultrascan II [23]. The K_d was determined for NrfA and the NrfA–NrfB complex assuming monomeric molecular masses of 53 and 74 kDa respectively. The molecular mass shown for NrfA–NrfB samples is the averaged molecular mass determined at the two different speeds.

Sample (μM)	λ (nm)	ε ($mM^{-1} \cdot cm^{-1}$)	Averaged molecular mass (kDa)	K_d (μM)
NrfA (2.0)	410	497	72	
NrfA (10)	440	110	83	4.0
NrfA (20)	530	48	98	
NrfA–NrfB (1.0)	410	1000	97 ± 4	
NrfA–NrfB (5.0)	530	96	134 ± 1	4.2
NrfA–NrfB (20)	600	15	147 ± 9	

conditions, hydroxide or substrate on the distal side. Much of the homodimer interface is formed from a pair of long interacting helices, at the end of which, partially exposed to solvent, is haem 5. The distance between the haems 5, one from each NrfA monomer, is only 4 Å (edge to edge). This distance of separation shows that electrons could easily travel from one monomer to another by exchange through these haems [2]. In the present study, we have established the equilibrium dissociation constant for 2(NrfA) ↔ $NrfA_2$ and show that this is the same as for the 2(NrfA–NrfB) ↔ $NrfA_2$–$NrfB_2$ equilibrium. This suggests that the binding site on NrfA for NrfB does not overlap with the NrfA dimer interface. Such a site could be provided around NrfA haem 2, which is the most solvent-exposed haem [2]. Thus we feel that any model for electron transfer between NrfB and NrfA would have to bring NrfB haem 5 (the putative electron egress haem) to within 14 Å of NrfA haem 2.

While the present work was in progress, the structure of a $NrfA_4$–$NrfH_2$ complex for *D. vulgaris* was published [8]. In contrast with NrfA–NrfB, NrfH and NrfA form a very tight 'hard-wired' interaction, indeed NrfH has never been purified in a native form independently of its cognate NrfA. The crystal structure provides some insight into this tight interaction, since two of the NrfA proteins provide lysine ligands to one of the haems on each NrfH protein in the $NrfA_4$–$NrfH_2$ complex. We have not been able to purify a NrfA–NrfB complex or co-crystallize such a complex, but, as discussed above, our solution-state protein–protein interaction studies strongly suggest that NrfA and NrfB form a 2:2 complex that will be structurally distinct from the $NrfA_4$–$NrfH_2$ complex. However, our structure of NrfB also reveals that NrfH and NrfB are structurally distinct in many ways so that there is no reason to expect *a priori* that the NrfA–NrfB and NrfA–NrfH stoichiometries should be the same. For example: (i) the sequence identity between NrfB and NrfH proteins is very low (~15%) and this is largely contributed to by alignment of four CXXCH motifs (see Supplementary Figure S1); (ii) NrfH has a transmembrane helix located towards the N-terminus, whereas NrfB is a soluble periplasmic protein in which the N-terminal signal peptide has been cleaved; and (iii) the polypeptide chain of

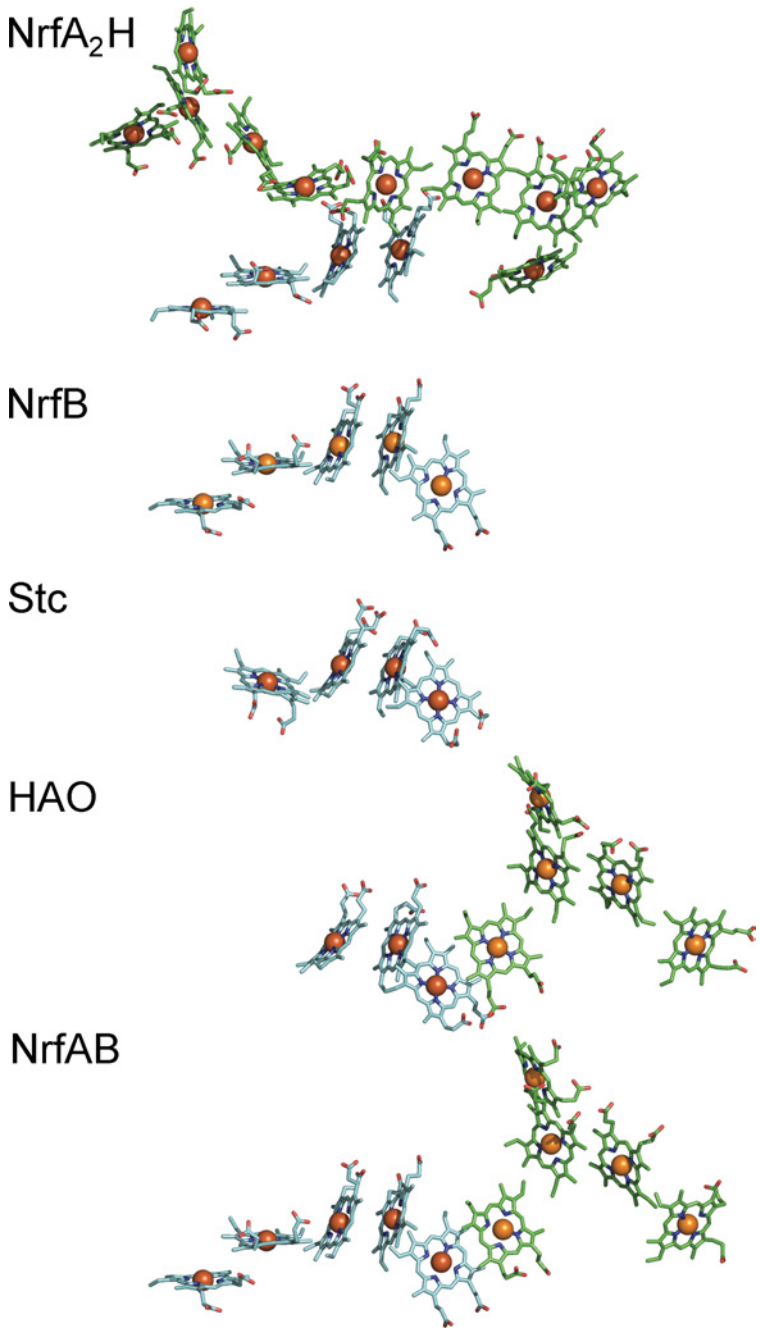

Figure 5 Comparison of the haem packing motifs of NrfB and NrfA (PDB code 1GU6) with $NrfA_2H$ (PDB code 2J7A), HAO (PDB code 1FGJ) and STC (PDB code 1M1Q)

In the case of the putative NrfA–NrfB complex, the NrfB haems are shown in blue, the NrfA haems are shown in green and the numbers denote NrfA haems 2 and 5. Dimerization of NrfA occurs at the haem 5 interface (see Supplementary Figure S1 at http://www.BiochemJ.org/bj/406/bj4060019add.htm).

NrfB and the soluble domain of NrfH can not be superimposed. Despite this, four of the NrfB haems (haems 1–4) adopt similar haem–haem packing motifs to the four NrfH haems (Figure 5) and can be superimposed with an rmsd of 1.93 Å. However, two of these four superimposable haems have different haem iron ligation. In NrfB, all five haem irons are low-spin hexaco-ordinate with bis-histidinyl axial ligation. However, in the $NrfA_4$–$NrfH_2$ complex, NrfH haem 1 is pentaco-ordinate (and therefore likely to be high-spin) with a methionine distal ligand and an aspartate residue occupying the proximal position, but not being within bonding distance. NrfH haem 4 is ligated by His^{140} provided by NrfH and Lys^{331} from NrfA. Although we are unable to provide a structure of NrfB in complex with NrfA, it should be noted that the EPR spectrum of a $NrfA_2$–$NrfB_2$ complex is simply the sum of the NrfA and NrfB spectra and thus does not indicate that any substantial change occurs in haems visible by EPR on complex formation (results not shown). A change to the EPR spectra would be indicative of either changes in haem co-ordination, such as a change from His-His to His-Met, or ligand orientation such as movement of the planar imidazole rings from a perpendicular to

a parallel arrangement. As no such changes are observed in the EPR spectrum of the $NrfA_2$–$NrfB_2$ complex, it seems likely that the environment of the NrfA and NrfB haems remains constant during complex formation.

The major difference between NrfB and NrfH is the presence of haem 5 in NrfB that is absent in the tetrahaem NrfH (see Supplementary Figure S1). This haem is the most likely electron-output site for NrfB, and its presence makes the construction of a NrfA–NrfB complex model using a NrfA–NrfH structural template impossible. However, it is notable that the position of NrfB haem 5 has equivalents in some other multihaem cytochrome systems. One of these is the 12 kDa STC (small tetrahaem cytochrome *c*) of *Shewanella* spp. that is involved in periplasmic electron transfer and respiration on soluble Fe(III) [25]. Haems 1–4 of STC overlay on to haems 2–5 of NrfB with an rmsd of 1.20 Å (Figure 5), which reveals clear similarities between these two small periplasmic electron-transfer proteins. Perhaps more intriguing, however, it has been noted previously that haems 1–5 of NrfA can be superimposed on to the haems 4–8 of the octahaem HAO (hydroxylamine oxidoreductase) subunit with an rmsd of 1.1 Å [3,26]. We can now show that the remaining haems 1–3 of HAO can be superimposed on to haems 3–5 of NrfB with an rmsd of 1.46 Å (Figure 5). This introduces the possibility that the octahaem HAO polypeptide, rather than the NrfH–NrfA complex, may provide a better conceptual template for a model for the NrfA–NrfB arrangements. Such a model would be consistent with the suggestion raised earlier that NrfB might dock on to NrfA such that NrfB haem 5 approaches NrfA haem 2 (Figure 5). Previously, NrfA haem 2 was identified as the site of electron input into NrfA [2] owing to a conserved region in NrfA sequences which employ NrfB as an electron donor. This conserved region is absent in NrfA proteins that use NrfH as an electron donor. It should be noted that, to achieve the HAO-type of haem arrangement for NrfA–NrfB, a rearrangement of the NrfA structure involving two flexible α-helices located at the surface near haem 2 (see Supplementary Figure S1) would be required. These structural elements have temperature factors that are among the highest for residues in the NrfA structure and are therefore predicted to be mobile. A number of significant structural changes also occur in the NrfH-dependent NrfA proteins on binding NrfH, and so a degree of structural re-arrangement of NrfB-dependent NrfA on binding NrfB cannot be excluded.

In closing this discussion of the NrfB structure, we move away from electron egress from haem 5 and the interaction with NrfA to consider electron input. Haem 1 of NrfB superimposes on to haem 1 of NrfH (Figure 5). In NrfH, this is the probable primary acceptor haem for electrons extracted from quinol through the quinol dehydrogenase activity of the protein. It is also then reasonable to argue that this is the most likely electron input site in NrfB. However, NrfB is not a quinol dehydrogenase. Unlike the $NrfA_4$–$NrfH_2$ electron transport complex that binds a complete 'quinol-to-nitrite' electron transport chain, the $NrfA_2$–$NrfB_2$ complex has to be interfaced to the quinol pool by yet another redox protein complex, the NrfC–NrfD complex, that is predicted to bind four iron–sulfur clusters. Thus the crystal structure of this complex is required before the full 'quinol-to-nitrite' electron transport chain of the NrfB-dependent cytochrome *c* nitrite reductase system can be fully understood.

We are grateful to Ann Reilly and Christine Moore for excellent technical support and to Dr Jörg Simon, Dr Julea Butt, Dr Myles Cheesman and Dr James Gwyer for helpful discussions. This work was supported by BBSRC (Biotechnology and Biological Sciences Research Council) grant B18695 to D. J. R., A. M. H. and J. A. C., Wellcome Trust JIF (Joint Infrastructure Funding) grant 0162178 to D. J. R. and A. M. H., and the U.S. Department of Energy Office of Biological and Environmental Research under the Genomics-Genomes to Life Program and an EMSL (Environmental Molecular Science Laboratory) Scientific Grand Challenge project.

REFERENCES

1 Poock, S. R., Leach, E. R., Moir, J. W., Cole, J. A. and Richardson, D. J. (2002) Respiratory detoxification of nitric oxide by the cytochrome *c* nitrite reductase of *Escherichia coli*. J. Biol. Chem. **277**, 23664–23669
2 Bamford, V. A., Angove, H. C., Seward, H. E., Thomson, A. J., Cole, J. A., Butt, J. N., Hemmings, A. M. and Richardson, D. J. (2002) Structure and spectroscopy of the periplasmic cytochrome *c* nitrite reductase from *Escherichia coli*. Biochemistry **41**, 2921–2931
3 Einsle, O., Messerschmidt, A., Stach, P., Bourenkov, G. P., Bartunik, H. D., Huber, R. and Kroneck, P. M. (1999) Structure of cytochrome *c* nitrite reductase. Nature **400**, 476–480
4 Einsle, O., Stach, P., Messerschmidt, A., Simon, J., Kroger, A., Huber, R. and Kroneck, P. M. (2000) Cytochrome *c* nitrite reductase from *Wolinella succinogenes*: structure at 1.6 Å resolution, inhibitor binding, and heme-packing motifs. J. Biol. Chem. **275**, 39608–39616
5 Cuhna, C. A., Macieira, S., Dias, J. M., Almeida, G., Gonçalves, L. L., Costa, C., Lampreia, J., Huber, R., Moura, J. J. G., Moura, I. and Romão, M. J. (2003) Cytochrome *c* nitrite reductase from *Desulfovibrio desulfuricans* ATCC 27774: the relevance of the two calcium sites in the structure of the catalytic subunit (NrfA). J. Biol. Chem. **278**, 17455–17465
6 Simon, J. (2002) Enzymology and bioenergetics of respiratory nitrite ammonification. FEMS Microbiol. Rev. **26**, 285–309
7 Schumacher, W., Hole, U. and Kroneck, P. M. H (1994) Ammonia-forming cytochrome *c* nitrite reductase from *Sulfurospirillum deleyianum* is a tetraheme protein: new aspects of the molecular composition and spectroscopic properties. Biochem. Biophys. Res. Commun. **205**, 911–916
8 Rodriques, M. L., Oliveira, T. F., Pereira, I. A. C. and Archer, M. (2006) X-ray structure of the membrane-bound cytochrome *c* quinol dehydrogenase NrfH reveals novel haem coordination. EMBO J. **25**, 5951–5960
9 Clarke, T. A., Dennison, V., Seward, H., Burlat, B., Cole, J. A., Hemmings, A. M. and Richardson, D. J. (2004) Purification and spectropotentiometric characterization of *Escherichia coli* NrfB, a decaheme homodimer that transfers electrons to the decaheme periplasmic nitrite reductase complex. J. Biol. Chem. **279**, 41333–41339
10 Potter, L. C. and Cole, J. A. (1999) Essential roles for the products of the *napABCD* genes, but not *napFGH*, in periplasmic nitrate reduction by *Escherichia coli* K-12. Biochem. J. **344**, 69–76
11 Leslie, A. G. W. (1992) Recent changes to the MOSFLM package for processing film and image plate data, Joint CCP4 + ESF-EAMCB Newsletter on Protein Crystallography, no. 26
12 Evans, P. (2006) Scaling and assessment of data quality. Acta Crystallogr. Sect. D. Biol. Crystallogr. **62**, 72–82
13 Collaborative Computational Project, Number 4 (1994) The CCP4 suite: programs for protein crystallography. Acta Crystallogr. Sect. D Biol. Crystallogr. **50**, 760–763
14 Sheldrick, G. M. (1990) Phase annealing in *SHELX*-90: direct methods for larger structures. Acta Crystallogr. Sect. A Found. Crystallogr. **46**, 467–473
15 Emsley, P. and Cowtan, K. (2004) Coot: model-building tools for molecular graphics. Acta Crystallogr. Sect. D. Biol. Crystallogr. **60**, 2126–2132
16 Bricogne, G., Vonrhein, C., Flensburg, C., Schiltz, M. and Paciorek, W. (2003) Generation, representation and flow of phase information in structure determination: recent developments in and around SHARP 2.0. Acta Crystallogr. Sect. D Biol. Crystallogr. **59**, 2023–2030
17 Brünger, A. T., Adams, P. D., Clore, G. M., DeLano, W. L., Gros, P., Grosse-Kunstleve, R. W., Jiang, J.-S., Kuszewski, J., Nilges, M., Pannu, N. S. et al. (1998) Crystallography & NMR system: a new software suite for macromolecular structure determination. Acta Crystallogr. Sect. D. Biol. Crystallogr. **54**, 905–921
18 Brünger, A. T. (1992) Free R value: a novel statistical quantity for assessing the accuracy of crystal structures. Nature **355**, 472–475
19 Murshudov, G. N., Vagin, A. A. and Dodson, E. J. (1997) Refinement of macromolecular structures by the maximum-likelihood method. Acta Crystallogr. Sect. D Biol. Crystallogr. **53**, 240–255
20 Cohen, S. X., Morris, R. J., Fernandez, F. J., Jelloul, M. B., Kakaris, M., Parthasarathy, V., Lamzin, V. S., Kleywegt, G. J. and Perrakis, A. (2004) Towards complete validated models in the next generation of *ARP/wARP*. Acta Crystallogr. Sect. D Biol. Crystallogr. **60**, 2222–2229
21 Laskowski, R. A., MacArthur, M. W., Moss, D. S. and Thornton, J. M. (1993) PROCHECK: a program to check the stereochemical quality of protein structures. J. Appl. Crystallogr. **26**, 283–291
22 Vagin, A. and Teplyakov, A. (2000) An approach to multi-copy search in molecular replacement. Acta Crystallogr. Sect. D. Biol. Crystallogr. **56**, 1622–1624

23 Demeler, B. (2005) UltraScan: a comprehensive data analysis software package for analytical ultracentrifugation experiments. In Modern Analytical Ultracentrifugation: Techniques and Methods (Scott, D. J., Harding, S. E. and Rowe, A. J., eds), pp. 210–229, Royal Society of Chemistry, London
24 Walker, F. A. (1999) Magnetic spectroscopic (EPR, ESEEM, Mössbauer, MCD and NMR) studies of low-spin ferriheme centers and their corresponding heme proteins. Coord. Chem. Rev. **186**, 471–534
25 Leys, D., Meyer, T. E., Tsapin, A. S., Nealson, K. H., Cusanovich, M. A. and Van Beeumen, J. J. (2002) Crystal structures at atomic resolution reveal the novel concept of "electron-harvesting" as a role for the small tetraheme cytochrome *c*. J. Biol. Chem. **277**, 35703–35711
26 Igarashi, N., Morigama, H., Fujiwara, T., Fukomon, Y. and Tanaka, N. (1997) The 2.8 Å structure of hydroxylamine oxidoreductase from a nitrifying chemoautotrophic bacterium, *Nitrosomonas europaea*. Nat. Struct. Biol. **4**, 276–289

Received 5 March 2007/18 May 2007; accepted 23 May 2007
Published as BJ Immediate Publication 23 May 2007, doi:10.1042/BJ20070321